

Understanding electron behavior in strained graphene as a reciprocal space distortion

M. Oliva-Leyva* and Gerardo G. Naumis†

*Departamento de Física-Química, Instituto de Física,
Universidad Nacional Autónoma de México (UNAM),
Apartado Postal 20-364, 01000 México, Distrito Federal, México*

The behavior of electrons in strained graphene is usually described using effective pseudomagnetic fields in a Dirac equation. Here we consider the particular case of a spatially constant strain. Our results indicate that lattice corrections are easily understood using a strained reciprocal space, in which the whole energy dispersion is simply shifted and deformed. This leads to a directional dependent Fermi velocity without producing pseudomagnetic fields. The corrections due to atomic wavefunction overlap changes tend to compensate such effects. Also, the analytical expressions for the shift of the Dirac points, which do not coincide with the K points of the renormalized reciprocal lattice, as well as the corresponding Dirac equation are found. In view of the former results, we discuss the range of applicability of the usual approach of considering pseudomagnetic fields in a Dirac equation derived from the old Dirac points of the unstrained lattice or around the K points of the renormalized reciprocal lattice. Such considerations are important if a comparison is desired with experiments or numerical simulations.

PACS numbers: 73.22.Pr, 81.05.ue

I. INTRODUCTION

Since the experimental observation of graphene,¹ a two-dimensional form of carbon, there have been many theoretical and experimental studies to understand and take advantage of its surprising properties.^{2–5} Among its most interesting features, one can cite the peculiar interplay between its electronic and its mechanical properties. Graphene can withstand elastic deformations up to 20%, much more than in any other crystal.⁶ Needless to say, this long interval of elastic response results in strong changes in the electronic structure, which offers a new direction of exploration in electronics: strain engineering.^{7–10} The prospect is to explore mechanical deformations as a tool for controlling electrical transport in graphene devices: a technological challenge owing to the counterintuitive behavior of electrons as massless Dirac fermions.¹¹

The most popular model proposed in the literature for studying the concept of strain engineering is based on a combination of a tight-binding (TB) description of the electrons and linear elasticity theory.^{12–15} In this approach, where the absence of electron-electron interactions is assumed, the electronic implications of lattice deformations are captured by means of a pseudovector potential \mathbf{A} which is related to the strain tensor ϵ by¹⁵

$$A_x = \frac{\beta}{2a}(\epsilon_{xx} - \epsilon_{yy}), \quad A_y = -\frac{\beta}{2a}(2\epsilon_{xy}), \quad (1)$$

where $a \approx 1.42 \text{ \AA}$ is the unstrained carbon-carbon distance (see FIG. 1 (a)) and $\beta \approx 3$ modulates the variation of the hopping energy t of the TB model with the changes in the intercarbon distance due to lattice deformations.^{4,7} Note that, the x axis is selected parallel to the zigzag direction. This β -dependent pseudovector potential gives a coupling of the pseudomagnetic field

($\mathbf{B} = \nabla \times \mathbf{A}$) with the electronic density. The idea of pseudomagnetic fields has been key in the understanding of the pseudo Landau levels experimental observations made in strained graphene, which had been theoretically predicted earlier.^{16,17}

In recent works, the standard description of the strain-induced vector field has been supplemented with the explicit inclusion of the local deformation of the lattice vectors.^{18–22} After accounting for the actual atomic positions to the TB Hamiltonian, Kitt *et al.* proposed an extra pseudovector potential which is β -independent and different at each of the strained Dirac points.¹⁸ The possible physical relevance of the extra β -independent term, predicted in the work of Kitt *et al.*, was discussed by de Juan *et al.* within the TB approach.¹⁹ They also obtained an extra β -independent pseudovector potential but with zero curl. Therefore, they concluded that in strained graphene no β -independent pseudomagnetic field exist.^{19,20}

The controversy created by Kitt *et al.* has also been solved in Refs. 21 and 22, where the concept of renormalization of the reciprocal space was a core and novel idea developed to meet that end. However, as has been documented in Ref. 7, the positions of the energy minima and maxima (Dirac points) do not coincide with the high-symmetry points at the corners of the renormalized Brillouin zone (e.g., the K point in FIG. 1 (c)). This last statement motivates us to seek the effective Hamiltonian around the Dirac points using such renormalization, since, as shown here, this is essential to understand the experimental data.

In this paper we analyze the most simple case, a spatially uniform strain. The reason is that such a case must be contained as a limiting case in any of the general theories, and at the same time, as shown here, it can be solved exactly. Thus, it is an important benchmark tool

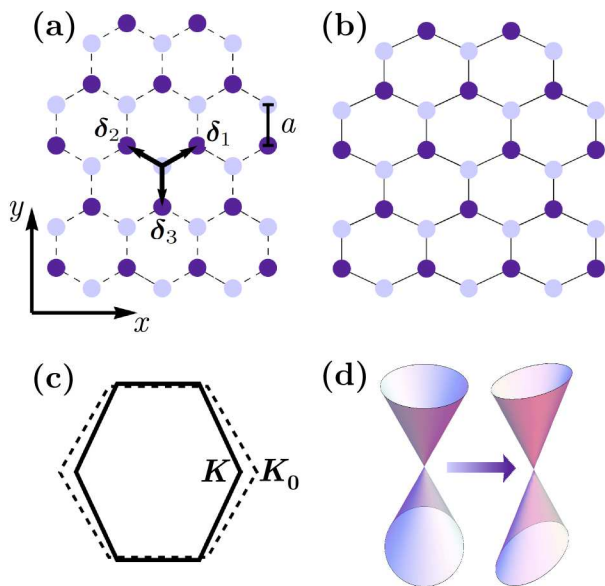


FIG. 1. (Color online) (a) Unstrained graphene lattice showing the vectors δ_i that point to the neighbors of type A sites, (b) the same lattice under a uniform stress, and (c), the first Brillouin zone of the reciprocal lattice for unstrained (dashed lines) and strained (solid lines) graphene. Note how the reciprocal lattice is contracted in the direction where the lattice is stretched, and the change of the \mathbf{K}_0 symmetry point into \mathbf{K} . (d) How the distortion of the reciprocal lattice transform the original Dirac cone (left) into a distorted one (right) with a directional dependent Fermi velocity.

to compare and discriminate the goodness of previous approaches. For example, this leads to a simple explanation for the lattice correction terms and direction dependent Fermi velocity, since both are due to the effects of strain in reciprocal space. Hopefully, this will help to derive the consequences of lattice corrections of flexural modes or curved graphene. The layout of this work is the following. In Sec. II we present the model and find the corresponding energy dispersion surface. In Sec. III, we discuss the properties of the energy dispersion and find the analytical expressions for the shift of the Dirac points and the strained Dirac Hamiltonian. Section IV deals with the problem of how the usual pseudomagnetic fields approach needs to be added with some requirements in order to compare experiments and simulations. Finally, in the last section, our conclusions are given.

II. MODEL: ELASTICITY & TIGHT-BINDING

We are interested in uniform planar strain situations, i.e., the components of two-dimensional strain tensor ϵ are assumed to be position-independent. In this case, the displacement vector $\mathbf{u}(\mathbf{x})$ is given by $\mathbf{u}(\mathbf{x}) = \epsilon \cdot \mathbf{x}$, and therefore, the actual position of an atom $\mathbf{x}' = \mathbf{x} + \mathbf{u}(\mathbf{x})$ can be written as $\mathbf{x}' = (I + \epsilon) \cdot \mathbf{x}$, I being the 2×2 identity

matrix. In general, if \mathbf{r} represents a general vector in the unstrained graphene lattice, its strained counterpart is given by the relationship $\mathbf{r}' = (I + \epsilon) \cdot \mathbf{r}$.

We investigate the electronic implications of strain by means of the nearest-neighbor tight-binding Hamiltonian,

$$H = - \sum_{\mathbf{x}', n} t_{\mathbf{x}', n} a_{\mathbf{x}'}^\dagger b_{\mathbf{x}'+\delta'_n} + \text{H.c.}, \quad (2)$$

where \mathbf{x}' runs over all sites of the deformed A sublattice and δ'_n are the three nearest neighbor vectors. The operators $a_{\mathbf{x}'}$ and $b_{\mathbf{x}'+\delta'_n}$ correspond to creating and annihilating electrons on the sublattices A and B , at sites \mathbf{x}' and $\mathbf{x}'+\delta'_n$, respectively. The dispersion relation arise upon writing Eq. (2) in the momentum space. For this purpose, we replace the creation/annihilation operators by their Fourier expansions²³

$$a_{\mathbf{x}'}^\dagger = \frac{1}{\sqrt{N}} \sum_{\mathbf{k}_1} e^{i\mathbf{k}_1 \cdot (\mathbf{x} + \mathbf{u}(\mathbf{x}))} a_{\mathbf{k}_1}^\dagger, \quad (3a)$$

$$b_{\mathbf{x}'+\delta'_n} = \frac{1}{\sqrt{N}} \sum_{\mathbf{k}_2} e^{-i\mathbf{k}_2 \cdot (\mathbf{x} + \delta_n + \mathbf{u}(\mathbf{x} + \delta_n))} b_{\mathbf{k}_2}, \quad (3b)$$

where N is the number of elementary cells. In Eq. (2) we have written the hopping integral $t_{\mathbf{x}', n}$ as position-dependent, but in the considered case (uniform strain), it does not depend on the position, only on the direction: $t_{\mathbf{x}', n} = t_n$.

Under these considerations, calculation of the Hamiltonian in the \mathbf{k} -space is fairly straightforward, H becomes

$$H = - \sum_{\mathbf{k}, n} t_n e^{-i\mathbf{k} \cdot (I + \epsilon) \cdot \delta_n} a_{\mathbf{k}}^\dagger b_{\mathbf{k}} + \text{H.c.} \quad (4)$$

From this equation, it follows that the dispersion relation of graphene under spatially uniform strain is

$$E(\mathbf{k}) = \pm | \sum_n t_n e^{-i\mathbf{k} \cdot (I + \epsilon) \cdot \delta_n} |, \quad (5)$$

which is a closed expression for the energy. This equation provides a benchmark tool case for testing any Hamiltonian concerning strain in graphene, and suggests the procedure that is developed in the following section. If in Eq. (5), we define an auxiliary reciprocal vector $\mathbf{k}^* = (I + \epsilon) \cdot \mathbf{k}$, the dispersion relationship is almost equal to the case in unstrained graphene, except for the different values of t_n as a function of n . When such hopping changes are not considered, as explained in the following section, one gets that,

$$E(\mathbf{k}) = \pm | \sum_n t_0 e^{-i\mathbf{k}^* \cdot \delta_n} |, \quad (6)$$

which is exactly the same Hamiltonian as for unstrained graphene but now with \mathbf{k} replaced with \mathbf{k}^* . Here, no approximations are used and the spectrum can be obtained for all values of \mathbf{k}^* . If this Hamiltonian develops around the corresponding Dirac point, it is obvious

that the same Dirac Hamiltonian observed in unstrained graphene will appear (see below), with \mathbf{k} replaced with \mathbf{k}^* . This suggests doing a renormalization of the reciprocal space as performed in the next section, a result that was also found in Refs. 21 and 22. Furthermore, Eq. (5) can be numerically evaluated to test any effective Hamiltonian obtained by developing around particular points in k space.

It is important to remark that in the general case of a non-uniform strain, δ'_n are not given by $\delta'_n = (I + \epsilon) \cdot \delta_n$. In this case, $\epsilon(\mathbf{x})$ needs to be replaced by the displacement gradient tensor $\nabla \mathbf{u}$.^{20,24} See in Ref. 20 how the use of $\delta'_n = (I + \nabla \mathbf{u}) \cdot \delta_n$, allowed Kitt *et al.* to solve the controversy concerning whether or not lattice corrections produce pseudovector potentials.

III. ENERGY SPECTRUM OF STRAINED GRAPHENE

The variation of the hopping energy t_n with the changes in the intercarbon distance fulfills a physically accurate exponential decay $t_n = t_0 \exp[-\beta(|\delta'_n|/a - 1)]$, with $t_0 \simeq 2.7$ eV being the equilibrium hopping energy.^{4,25} Nevertheless, for the sake of comparison with previous works we consider first order in strain,

$$t_n \simeq t_0 \left(1 - \frac{\beta}{a^2} \delta_n \cdot \epsilon \cdot \delta_n\right). \quad (7)$$

Defining the three nearest neighbor vectors as depicted in FIG. 1,

$$\delta_1 = \frac{a}{2}(\sqrt{3}, 1), \quad \delta_2 = \frac{a}{2}(\sqrt{3}, 1), \quad \delta_3 = a(0, -1), \quad (8)$$

and plugging Eq. (7) into Eq. (5), one gets the following expression for the dispersion relation,

$$E(\mathbf{k}) = \pm t_0 \sqrt{3 + f(\mathbf{k}^*) - \beta(3\text{Tr}(\epsilon) + f_\epsilon(\mathbf{k}^*)) + \beta^2 f_{\epsilon^2}(\mathbf{k}^*)}, \quad (9)$$

where $f(\mathbf{k}^*)$ has exactly the same functional form of its unstrained graphene counterpart,⁴

$$f(\mathbf{k}^*) = 2 \cos(\sqrt{3}k_x^* a) + 4 \cos\left(\frac{\sqrt{3}k_x^* a}{2}\right) \cos\left(\frac{3k_y^* a}{2}\right), \quad (10)$$

but now evaluated in different points of reciprocal space, since here $\mathbf{k}^* = (k_x^*, k_y^*)$ is given by the transformation,

$$\mathbf{k}^* = (I + \epsilon) \cdot \mathbf{k}. \quad (11)$$

This last equation is very important. It provides a mapping of the original reciprocal space into a new distorted one. As we will see, this mapping and the fact that $f(\mathbf{k}^*)$ is equal to its undistorted counterpart lead to pure geometrical effects that only very recently have been identified.¹⁸⁻²² The other terms depend on the same distortion, but contain hopping corrections. These terms are explicitly detailed in the Appendix A. $f_\epsilon(\mathbf{k}^*)$ contains the modification of the spectrum due to first order in β , while $f_{\epsilon^2}(\mathbf{k}^*)$ is the second order correction in β .

A. Hypothetical case: $\beta = 0$

Several important consequences follow from these equations. First of all, one can observe that in the case of deforming the lattice without changing the hopping parameters, i.e., if one deforms the lattice keeping $\beta = 0$, $E(\mathbf{k})$ is simplified to:

$$E(\mathbf{k}) = \pm t_0 \sqrt{3 + f(\mathbf{k}^*)}. \quad (12)$$

This corresponds to the same dispersion relationship observed in graphene, but now with different reciprocal vectors, which are obtained by applying strain to the original reciprocal vectors. In other words, the space is strained while the eigenvalues remain the same. As a consequence, the Dirac cone changes its shape due to this lattice deformation, as illustrated in FIG. 1. This is exactly the result that we would obtain if a diagonalization of the tight-binding Hamiltonian is performed using a computer. Since $\beta = 0$ and the connectivity of the lattice is not changed, the eigenvalues of the Hamiltonian must remain equal to the undistorted case. Only when a plot is made *against the wavevectors*, the cone turns out to be distorted, as shown in FIG. 1 (d). For example, the brick wall lattice has the same connectivity as graphene, and thus the spectrum must be the same. However, only when the spectrum is plotted in reciprocal space, the energy-momentum relationship appears distorted.

Also, the case $\beta = 0$ allows us to appreciate a subtle point. Since the spectrum is the same as in unstrained graphene, it is easy to see that the \mathbf{K} symmetry points of the distorted lattice coincide with the Dirac point of the new relationship given by Eq. (12). In other words, the condition $E(\mathbf{K}_D) = 0$, which defines the \mathbf{K}_D Dirac points, corresponds to $\mathbf{K}_D = \mathbf{K}$, where \mathbf{K} is the image of the point \mathbf{K}_0 under the mapping $\mathbf{K} = (I + \epsilon)^{-1} \cdot \mathbf{K}_0$. Thus, for $\beta = 0$ it makes sense to develop the TB Hamiltonian around the original Dirac points, as $\mathbf{k} = \mathbf{K}_D + \mathbf{q}$, with $|\mathbf{q}| \ll |\mathbf{K}_D|$. It is easy to show that the pure geometrical distortion allows us to write the Dirac Hamiltonian as (see Appendix B),

$$H = v_0 \boldsymbol{\sigma} \cdot (I + \epsilon) \cdot \mathbf{q} = v_0 \boldsymbol{\sigma}' \cdot \mathbf{q}, \quad (13)$$

\mathbf{q} being the momentum measured relatively to the Dirac points, $v_0 = 3t_0 a/2$ the Fermi velocity for the undeformed lattice, $\boldsymbol{\sigma} = (\sigma_x, \sigma_y)$ the two Pauli matrices and $\boldsymbol{\sigma}' = (I + \epsilon) \cdot \boldsymbol{\sigma}$ turns out to be the spinorial connection.²⁶ From this equation follows a directional dependent Fermi velocity for strained graphene, which has also been found in other works.^{7,19} Furthermore, a directional dependent velocity appears simply by looking at the isoenergetic curves of Eq. (12) around \mathbf{K} . In this case one obtains

$$E(\mathbf{K} + \mathbf{q})^2 = (v_0 \boldsymbol{\sigma} \cdot (I + \epsilon) \cdot \mathbf{q})^2, \quad (14)$$

therefore, the isoenergetic curves around \mathbf{K} are rotated ellipses, as depicted in FIG. 2 (b). This figure was made for a zigzag uniaxial strain of 5%, i.e., $\epsilon_{xx} = 0.05$, $\epsilon_{xy} = 0$

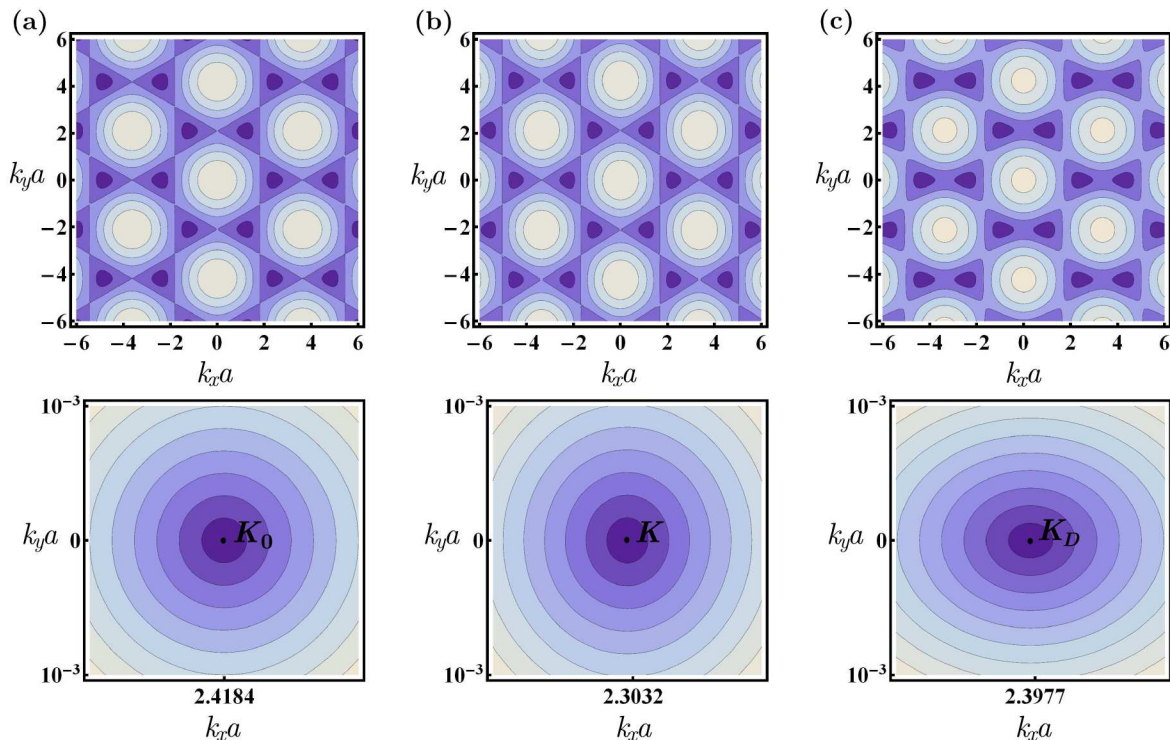


FIG. 2. (Color online) Isoenergetic curves obtained from the energy dispersion in reciprocal space obtained from Eq. (9). A blow up is presented around the Dirac points \mathbf{K}_D for each surface. Case (a) corresponds to unstrained graphene, (b) to strained graphene with $\beta = 0$, $\epsilon_{xx} = 0.05$, $\epsilon_{xy} = 0$, $\epsilon_{yy} = -\nu\epsilon_{xx}$, and (c) to strained graphene with $\beta \approx 3$, and the same strain tensor as in case (b). Note how although the strain tensor is the same in cases (b) and (c), the ellipses are rotated by $\pi/2$, since the reciprocal space deformation and hopping effects tend to compensate.

and $\epsilon_{yy} = -\nu\epsilon_{xx}$, ν being the Poisson ratio, which is very low for graphene, $\nu \sim 0.1 - 0.15$, according to some theoretical estimations.^{27,28}

At this point, one can conclude that the basic mechanism behind the anisotropic Fermi velocity is the distortion of the reciprocal space. Such distortion gives a simple interpretation to the resulting geometric crystal frame terms that appears in the covariant version of the equations.¹⁹ Clearly, there are not associated pseudomagnetic fields.^{7,19}

B. Actual case: $\beta \neq 0$

Let us now consider the case in which the space is distorted and the hopping is changed, i.e., $\beta \neq 0$. Here, we will have two effects. Again one has the pure geometrical distortion due to the strain of the reciprocal space, but at the same time, there is a change in the spectrum. This last effect is the only one observed when a diagonalization of the Hamiltonian is performed in a computer for a finite number of atoms.

In FIG. 2, a comparison between the cases $\beta = 0$ and $\beta \neq 0$ is presented for $E(\mathbf{k})$. As can be seen, the effect of $\beta \neq 0$ is to distort the $\beta = 0$ case in such a way that it tends to compensate the strain of the reciprocal

space, i.e., the ellipses are rotated by $\pi/2$ for a realistic value of β . The physical reason for this occurrence is that a stretched direction in real space shirks in reciprocal space, resulting in a higher Fermi velocity, while in the same direction, the orbital overlap decreases since the distance between atoms increases (see FIG. 1). This tends to reduce the Fermi velocity. As a result, lattice distortion and hopping changes tend to compensate. This fact can also be seen in the movement of the Dirac points. From the FIG. 2, one can see that the Dirac points for the case $\beta \neq 0$ are closer to the original ones than their $\beta = 0$ counterparts.

The qualitative results discussed above, and depicted in FIG. 2, can be understood by finding analytical expressions for \mathbf{K}_D and H . The position of \mathbf{K}_D can be obtained from the condition $E(\mathbf{K}_D) = 0$. Up to first order in strain, we obtained that \mathbf{K}_D is given as follows:

$$\mathbf{K}_D \simeq (I + \epsilon)^{-1} \cdot (\mathbf{K}_0 + \xi \mathbf{A}) \simeq \mathbf{K} + \xi \mathbf{A}, \quad (15)$$

with \mathbf{A} defined by Eq. (1) and ξ the valley index of \mathbf{K}_0 .²³ The previous equation confirms the remark that the Dirac points for $\beta \neq 0$ do not coincide with the \mathbf{K} high symmetry points of the strained Brillouin zone. The shift, which is only produced by β , is given by the pseudovector potential, and do not depend on \mathbf{K}_0 .

Furthermore, once the points \mathbf{K}_D are known, it is possible to obtain a new Dirac Hamiltonian considering the

lattice correction and orbital overlap changes. To do this, we developed Eq. (4) around the Dirac points using Eq. (15), and derived that (see Appendix C)

$$H = v_0 \boldsymbol{\sigma} \cdot (\mathbf{I} + \boldsymbol{\epsilon} - \beta \boldsymbol{\epsilon}) \cdot \mathbf{q}, \quad (16)$$

which is a general version of Eq. (13), since β effects are included. Notice that the isoenergetic curves around \mathbf{K}_D remain ellipses, as depicted in FIG. 2 (c), but with different values of the semi-axes owing to the β corrections. The last equation clearly shows the tendency of β to cancel the lattice corrections.

Let us make two important remarks about Eqs. (15) and (16), which are among the main contributions of this paper. First, these equations are a generalization of analogous expressions to the case of graphene under uniaxial strain which were inherited from studies on deformed carbon nanotubes.²⁹ Similar expressions were also found for a particular case of distortion without shear. Thus, our generalization can be reduced to other special cases for which the results are known,^{7,29,30} and coincides with the exact solvable case for $\beta = 0$. Such limiting cases allows us to check in different ways the validity of the presented results. Second, Eq. (16) can not be derived from the theory of the strain-induced pseudomagnetic field. Namely, the effective Dirac Hamiltonian obtained by this theory does not reduce to our Eq. (16) for the case of uniform strain, for reasons explained in the following section.

IV. EXPERIMENTAL OBSERVATION OF PSEUDOMAGNETIC FIELDS

From the point of view developed in the previous section, it is clear that basically, the Dirac cone is translated and distorted. As a result, if one tries to derive an effective Dirac equation using \mathbf{K}_0 as starting points to develop $E(\mathbf{k})$ as $\mathbf{k} = \mathbf{K}_0 + \mathbf{q}$, the resulting energy can be quite far away from the Fermi energy, as shown in FIG. 3. This poses a problem that has been overlooked in the usual treatment of strain in graphene using pseudomagnetic fields in the Dirac equations.

In general, if Eq. (9) is developed around a general point in reciprocal space given by \mathbf{K}_G , we get,

$$E^2(\mathbf{K}_G + \mathbf{q}) \simeq E^2(\mathbf{K}_G) + \nabla E^2(\mathbf{K}_G) \cdot \mathbf{q} + \frac{1}{2} \mathbf{q} \cdot \nabla \nabla E^2(\mathbf{K}_G) \cdot \mathbf{q}, \quad (17)$$

where $\nabla E^2(\mathbf{K}_G)$ is the Jacobian vector and $\nabla \nabla E^2(\mathbf{K}_G)$, the Hessian matrix of $E^2(\mathbf{k})$, which are evaluated at $\mathbf{k} = \mathbf{K}_G$.

In the usual procedure $\mathbf{K}_G = \mathbf{K}_0$. However, $E^2(\mathbf{K}_0) \neq 0$ and $\nabla E^2(\mathbf{K}_G) \neq 0$. This produces an energy shift and a \mathbf{q} dependent term, observed in other approaches,¹⁹ which complicates the description of the dynamics somehow.

This also poses an issue concerning the experimental possibility of observing the pseudomagnetic fields. Since the energy evaluated at the original Dirac point $E(\mathbf{K}_0)$ is

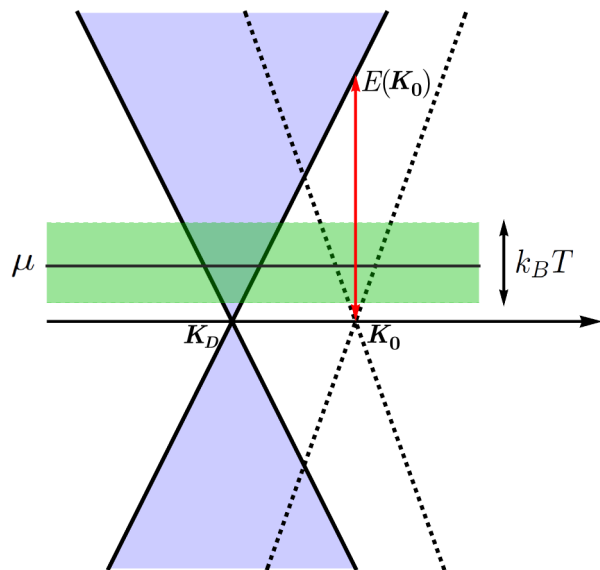


FIG. 3. (Color online) The Dirac cone in unstrained (dashed line) and strained graphene (solid line) and the experimental observation of electron behavior for a probe that shifts the chemical potential (μ) with respect to the Fermi energy. The shaded box indicates the width of the thermal selector due to the Fermi-Dirac distribution. The effective Dirac equation with pseudomagnetic fields can be obtained by developing around the original \mathbf{K}_0 points, or in the Dirac points \mathbf{K}_D of the strained lattice. For $\mu = 0$, only the latter approach will work for low temperatures.

different from zero, the Fermi energy does not fall at this point, as we illustrate in FIG. 3. In general, if an experiment is performed at temperature T , and the chemical potential μ is shifted by a field, the condition to observe the pseudomagnetic fields in the usual derivation around the original Dirac point must satisfy,

$$|E(\mathbf{K}_0) - \mu| \leq k_B T, \quad (18)$$

since the difference between $E(\mathbf{K}_0)$ and μ must be less than a zone defined from the derivative of the Fermi-Dirac distribution against the energy, as explained in FIG. 3 using a box around μ . As $T \rightarrow 0$, the derivative is a delta function centered around the Fermi energy, and the pseudomagnetic fields calculated from \mathbf{K}_0 are usually far from the region of validity. For example, even a zigzag uniaxial strain of 1%, will produce a $E(\mathbf{K}_0) \geq 27$ meV, which is much higher than the thermal width of $k_B T \approx 8.6$ meV, obtained at $T = 10$ K. This breaks the approximation of using pseudomagnetic fields in a Dirac equation unless a very well defined field is used.

The option is to have a better description of the energy dispersion near the Fermi energy, by developing Eq. (17) around the true Dirac points of the strained lattice, i.e., by setting $\mathbf{K}_G = \mathbf{K}_D$, for which the corresponding ener-

gies fall at the Fermi level. In this case,

$$E^2(\mathbf{K}_D + \mathbf{q}) \simeq \frac{1}{2} \mathbf{q} \cdot \nabla \nabla E^2(\mathbf{K}_D) \cdot \mathbf{q}, \quad (19)$$

since $E^2(\mathbf{K}_D) = 0$ and $\nabla E^2(\mathbf{K}_D) = 0$. Now one obtains an energy dispersion which corresponds to a distorted cone, with a directional dependent Fermi velocity given by the elements of the Hessian of $E^2(\mathbf{k})$ evaluated at \mathbf{K}_D . This result is the same as the one obtained from the Dirac Hamiltonian given by Eq. (16).

V. CONCLUSIONS

In conclusion, we have analyzed the case of a spatially uniform strain in graphene. The lattice correction terms are simply an effect of the strained reciprocal space. As a consequence, the Dirac cones are deformed and translated. No pseudomagnetic fields are associated to such terms, as has been recently discussed.^{7,19} When hopping changes are considered, there is an extra deformation of the cone that tends to cancel the effect of the reciprocal space strain. The new Dirac points of the strained Hamiltonian do not coincide with the \mathbf{K} symmetry points of the strained reciprocal lattice. Due to this fact, the effective Dirac equation can be obtained by developing around the old or the new Dirac points. If the old points are chosen,

as is usual in the graphene literature, there is a restriction to observe the dynamics produced by the calculated pseudomagnetic fields since only for very high temperatures or carefully designed probes is it possible to make a comparison with the usual theory. In computer simulations, it is also important to distinguish between lattice distortion effects and connectivity matrix. Some of these issues, can explain differences between theory and simulations in graphene.³¹

Finally, it is worth mentioning that although we only treated a particular case, the ideas and lessons obtained from this study can be translated to general cases, as we will show in forthcoming works.

ACKNOWLEDGMENTS

We are grateful to V. M. Pereira and B. B Goldberg for helpful discussions. This work was supported by UNAM-DGAPA-PAPIIT, project IN-102513. M.O.L acknowledges support from CONACYT (Mexico).

Appendix A

In this section, we provide explicit expressions for the last terms in Eq. (9),

$$\begin{aligned} f_\epsilon(\mathbf{k}^*) &= (3\epsilon_{xx} + \epsilon_{yy}) \cos(\sqrt{3}k_x^*a) + (3\epsilon_{xx} + 5\epsilon_{yy}) \cos\left(\frac{\sqrt{3}k_x^*a}{2}\right) \cos\left(\frac{3k_y^*a}{2}\right) - 2\sqrt{3}\epsilon_{xy} \sin\left(\frac{\sqrt{3}k_x^*a}{2}\right) \sin\left(\frac{3k_y^*a}{2}\right), \\ f_{\epsilon^2}(\mathbf{k}^*) &= \frac{1}{8}(9\epsilon_{xx}^2 + 6\epsilon_{xx}\epsilon_{yy} + 9\epsilon_{yy}^2 + 12\epsilon_{xy}^2 + ((3\epsilon_{xx} + \epsilon_{yy})^2 - 12\epsilon_{xy}^2) \cos(\sqrt{3}k_x^*) \\ &\quad + 8\epsilon_{yy}(3\epsilon_{xx} + \epsilon_{yy}) \cos(\sqrt{3}k_x^*/2) \cos(3k_y^*/2) - 16\sqrt{3}\epsilon_{yy}\epsilon_{xy} \sin(\sqrt{3}k_x^*/2) \sin(3k_y^*/2)). \end{aligned}$$

Appendix B

For the case $\beta = 0$, the hopping integral does not depend on the direction, $t_n = t_0$, and consequently the Hamiltonian TB given by Eq. (4) reduces to

$$H = -t_0 \sum_{\mathbf{k}, n} e^{-i\mathbf{k} \cdot (I + \epsilon) \cdot \delta_n} a_{\mathbf{k}}^\dagger b_{\mathbf{k}} + \text{H.c.}$$

The closed dispersion relation derived from this Hamiltonian has the form

$$E(\mathbf{k}) = \pm t_0 \sqrt{3 + f(\mathbf{k}^*)},$$

where $f(\mathbf{k}^*)$ is given by Eq. (10). As discussed in Section II, the condition $E(\mathbf{K}_D) = 0$, which defines the \mathbf{K}_D Dirac points, corresponds to $\mathbf{K}_D = \mathbf{K}$, where \mathbf{K} is the image of the point \mathbf{K}_0 under the mapping $\mathbf{K} = (I + \epsilon)^{-1} \cdot \mathbf{K}_0$. Thus, for $\beta = 0$ it makes sense to develop the TB

Hamiltonian around the original Dirac points, as $\mathbf{k} = \mathbf{K} + \mathbf{q}$, with $|\mathbf{q}| \ll |\mathbf{K}|$,

$$\begin{aligned} E(\mathbf{K} + \mathbf{q}) &= \pm t_0 \sqrt{3 + f((I + \epsilon) \cdot ((I + \epsilon)^{-1} \cdot \mathbf{K}_0 + \mathbf{q}))}, \\ &= \pm t_0 \sqrt{3 + f(\mathbf{K}_0 + (I + \epsilon) \cdot \mathbf{q})}, \\ &= \pm t_0 \sqrt{3 + f(\mathbf{K}_0 + \mathbf{q}^*)}, \quad \mathbf{q}^* = (I + \epsilon) \cdot \mathbf{q}, \\ &\simeq \pm v_0 |\mathbf{q}^*|, \\ &\simeq \pm v_0 |(I + \epsilon) \cdot \mathbf{q}|. \end{aligned}$$

In the next section we provide a more general proof of Eq. (13). At this point, is clear that the case $\beta = 0$ is a benchmark tool for any effective Hamiltonian, since it can be solved without using any approximation.

Appendix C

We start with the Hamiltonian in momentum space of strained graphene,

$$H = - \sum_{n=1}^3 t_n \begin{pmatrix} 0 & e^{-i\mathbf{k}\cdot(I+\epsilon)\cdot\boldsymbol{\delta}_n} \\ e^{i\mathbf{k}\cdot(I+\epsilon)\cdot\boldsymbol{\delta}_n} & 0 \end{pmatrix}, \quad (\text{C1})$$

where t_n is given by Eq. (7). Now, let us develop this Hamiltonian around an original Dirac point \mathbf{K}_D , which is defined by $\mathbf{K}_D = \mathbf{K} + \mathbf{A}$. Expanding $\mathbf{k} = \mathbf{K}_D + \mathbf{q}$ we get

$$H = - \sum_{n=1}^3 t_n \begin{pmatrix} 0 & e^{-i(\mathbf{K}_D+\mathbf{q})\cdot(I+\epsilon)\cdot\boldsymbol{\delta}_n} \\ e^{i(\mathbf{K}_D+\mathbf{q})\cdot(I+\epsilon)\cdot\boldsymbol{\delta}_n} & 0 \end{pmatrix}, \quad (\text{C2})$$

but $\mathbf{K}_D \cdot (I + \epsilon) \cdot \boldsymbol{\delta}_n = (\mathbf{K}_0 + \mathbf{A}) \cdot \boldsymbol{\delta}_n$, and to first order in \mathbf{q} and ϵ we may write

$$H \simeq - \sum_{n=1}^3 t_n \begin{pmatrix} 0 & e^{-i\mathbf{K}_0\cdot\boldsymbol{\delta}_n} \\ e^{i\mathbf{K}_0\cdot\boldsymbol{\delta}_n} & 0 \end{pmatrix} (1 - i\sigma_3 \mathbf{A} \cdot \boldsymbol{\delta}_n) (1 - i\sigma_3 \mathbf{q} \cdot (I + \epsilon) \cdot \boldsymbol{\delta}_n), \quad (\text{C3})$$

note that \mathbf{A} is an expression in the first order of strain. Using the following identity

$$\begin{pmatrix} 0 & e^{-i\mathbf{K}_0\cdot\boldsymbol{\delta}_n} \\ e^{i\mathbf{K}_0\cdot\boldsymbol{\delta}_n} & 0 \end{pmatrix} = i \frac{\boldsymbol{\sigma} \cdot \boldsymbol{\delta}_n}{a} \sigma_3, \quad (\text{C4})$$

$\boldsymbol{\sigma} = (\sigma_x, \sigma_y)$ being the two Pauli matrices, the Hamiltonian becomes

$$\begin{aligned} H &\simeq -t_0 \sum_{n=1}^3 \left(1 - \frac{\beta}{a^2} \boldsymbol{\delta}_n \cdot \epsilon \cdot \boldsymbol{\delta}_n\right) \left(i \frac{\boldsymbol{\sigma} \cdot \boldsymbol{\delta}_n}{a} \sigma_3\right) \left(1 - i\sigma_3 \mathbf{A} \cdot \boldsymbol{\delta}_n - i\sigma_3 \mathbf{q} \cdot (I + \epsilon) \cdot \boldsymbol{\delta}_n - (\mathbf{A} \cdot \boldsymbol{\delta}_n)(\mathbf{q} \cdot \boldsymbol{\delta}_n)\right), \\ &\simeq -t_0 \sum_{n=1}^3 \left(i \frac{\boldsymbol{\sigma} \cdot \boldsymbol{\delta}_n}{a} \sigma_3\right) \left(1 - i\sigma_3 \mathbf{q} \cdot (I + \epsilon) \cdot \boldsymbol{\delta}_n - (\mathbf{A} \cdot \boldsymbol{\delta}_n)(\mathbf{q} \cdot \boldsymbol{\delta}_n) + i \frac{\beta}{a^2} \sigma_3 (\boldsymbol{\delta}_n \cdot \epsilon \cdot \boldsymbol{\delta}_n)(\mathbf{q} \cdot \boldsymbol{\delta}_n) - i\sigma_3 \mathbf{A} \cdot \boldsymbol{\delta}_n - \frac{\beta}{a^2} \boldsymbol{\delta}_n \cdot \epsilon \cdot \boldsymbol{\delta}_n\right), \\ &\simeq v_0 \boldsymbol{\sigma} \cdot (I + \epsilon) \mathbf{q} - v_0 \boldsymbol{\sigma} \cdot \frac{\beta}{4} (2\epsilon - \text{Tr}(\epsilon)I) \cdot \mathbf{q} - v_0 \boldsymbol{\sigma} \cdot \frac{\beta}{4} (2\epsilon + \text{Tr}(\epsilon)I) \cdot \mathbf{q}, \\ &\simeq v_0 \boldsymbol{\sigma} \cdot (I + \epsilon - \beta\epsilon) \cdot \mathbf{q}. \end{aligned} \quad (\text{C5})$$

This is our Eq. (16), which also reproduces Eq. (13) for $\beta = 0$, therefore, this section can be taken as a proof of both equations: Eq. (13) and Eq. (16). It is important to emphasize that in this proof we assumed that the valley index of \mathbf{K}_0 is $\xi = 1$. For the case $\xi = -1$, the proof is

analogous, and the Hamiltonian is

$$H \simeq v_0 \boldsymbol{\sigma}^* \cdot (I + \epsilon - \beta\epsilon) \cdot \mathbf{q}, \quad (\text{C6})$$

with $\boldsymbol{\sigma}^* = (\sigma_x, -\sigma_y)$.

* moliva@fisica.unam.mx

† naumis@fisica.unam.mx

¹ K. S. Novoselov, A. K. Geim, S. V. Morozov, D. Jiang, Y. Zhang, S. V. Dubonos, I. V. Grigorieva, and A. A. Firsov, *Science* **306**, 666 (2004).

² A. K. Geim, *Science* **324**, 1530 (2009).

³ K. S. Novoselov, *Rev. Mod. Phys.* **83**, 837 (2011).

⁴ A. H. Castro Neto, F. Guinea, N. M. R. Peres, K. S. Novoselov, and A. K. Geim, *Rev. Mod. Phys.* **81**, 109 (2009).

⁵ S. Das Sarma et al., *Rev. Mod. Phys.* **83**, 407 (2011).

⁶ C. Lee, X. Wei, J. W. Kysar, and J. Hone, *Science* **321**, 385 (2008).

⁷ V. M. Pereira, A. H. Castro Neto, and N. M. R. Peres, *Phys. Rev. B* **80**, 045401 (2009).

⁸ V. M. Pereira, and A. H. Castro Neto, *Phys. Rev. Lett.* **103**, 046801 (2009).

⁹ F. Guinea, *Solid State Commun.* **152**, 1437 (2012).

¹⁰ Da Zhan, Jiayu Yan, Linfei Lai, Zhenhua Ni, Lei Liu, and Zexiang Shen, *Adv. Mater.* **24**, 4055 (2012).

¹¹ C. W. J. Beenakker, *Rev. Mod. Phys.* **80**, 1337 (2008).

¹² H. Suzuura, and T. Ando, *Phys. Rev. B* **65**, 235412 (2002).

¹³ J. L. Mañes, *Phys. Rev. B* **76**, 045430 (2007).

¹⁴ A. F. Morpurgo, and F. Guinea, *Phys. Rev. Lett.* **97**, 196804 (2006).

¹⁵ M. A. H. Vozmediano, M. I. Katsnelson, and F. Guinea, *Phys. Rep.* **496**, 109 (2010).

¹⁶ F. Guinea, M. I. Katsnelson, and A. K. Geim, *Nat. Phys.* **6**, 30 (2010).

¹⁷ F. Guinea, A. K. Geim, M. I. Katsnelson, and K. S. Novoselov, *Phys. Rev. B* **81**, 035408 (2010).

¹⁸ A. L. Kitt, V. M. Pereira, A. K. Swan, and B. B. Goldberg, *Phys. Rev. B* **85**, 115432 (2012).

¹⁹ F. de Juan, J. L. Mañes, and M. A. H. Vozmediano, *Phys. Rev. B* **87**, 165131 (2013).

- ²⁰ A. L. Kitt, V. M. Pereira, A. K. Swan, and B. B. Goldberg, Phys. Rev. B **87**, 159909(E) (2013).
- ²¹ J. V. Sloan, Alejandro A. P. Sanjuan, Z. Wang, C. Horvath, and S. Barraza-Lopez, Phys. Rev. B **87**, 155436 (2013).
- ²² S. Barraza-Lopez, A. A. P. Sanjuan, Z. Wang, and M. Vanevic Solid State Commun. **166**, 70 (2013).
- ²³ C. Bena, and G. Montambaux, New J. Phys. **11**, 095003 (2009).
- ²⁴ M. Ramezani Masir, D. Moldovan, F. M. Peeters, arXiv: 1304.0629.
- ²⁵ R. M. Ribeiro, V. M. Pereira, N. M. R. Peres, P. R. Bridgdon, and A. H. Castro Neto, New J. Phys. **11**, 115002 (2009).
- ²⁶ R. Kerner, G. G. Naumis, and W. Gómez-Arias, Phys. B: Condens. Matter, **407**, 2002 (2012).
- ²⁷ M. Farjam, and H. Rafii-Tabar, Phys. Rev. B **80**, 167401 (2009).
- ²⁸ K. V. Zakharchenko, M. I. Katsnelson, and A. Fasolino, Phys. Rev. Lett. **102**, 046808 (2009).
- ²⁹ L. Yang, and J. Han, Phys. Rev. Lett. **85**, 154 (2000).
- ³⁰ V. M. Pereira, R. M. Ribeiro, N. M. R. Peres, and A. H. Castro Neto, Europhys. Lett. **92**, 67001 (2010).
- ³¹ Y. Chang, T. Albash, and S. Haas, Phys. Rev. B **86**, 125402 (2012).